Spectrochimica Acta Part B 135 (2017) 73–81

Contents lists available at ScienceDirect

Spectrochimica Acta Part B

journal homepage: www.elsevier.com/locate/sab

Analysis of line profiles from transient plasmas using a pseudo-Fano function

Guido Baéz, Diego Díaz Pace*, Cristian D'Angelo, Héctor O. Di Rocco

Campus Universitario, (B7000GHG) Tandil, Buenos Aires, Argentina

ARTICLE INFO

Article history:
Received 6 April 2017
Received in revised form 6 July 2017
Accepted 10 July 2017
Available online 17 July 2017

1. Introduction

The spectral lines emitted by laboratory and astrophysical plasmas show variations with respect to its emissivity profile $\varepsilon(\omega)$ (proportional to the line shape factor $P(\omega)$, see Eq. (1)), due to the physical conditions (parameters) of the source [1]. For example 1) the full width at half maximum(FWHM) of the optically thin line is proportional to the electron density n_e, when it is broadened by the Stark effect[1], 2) if the emitting plasma core is surrounded by a colder one, the profile will show a dip at the line center [2], 3) when the ionic density n_i is important, the profile will show an asymmetry, specially for lines arising from higher levels [3], 4) specially, the asymmetry is also present in those profiles called "autoionizing" [4], 5) line shifts due to high electron densities can be observed [1]. All the above effects often occur simultaneously in plasmas produced by laser or high current pinch experiments.

In all the mentioned cases, it is paramount to recover the emissivity profile, in local thermodynamic equilibrium (LTE) or not [5]. In fact, the FWHM of the thin line is proportional to n_e (when Stark effect is dominant) and the ratio between integrated intensities is equal to the corresponding ratio of transition probabilities $I_{vu}/I_{po} \propto A_{vu}/A_{po}$ (in addition to a Boltzmann factor). Moreover, the emissivity line profiles are needed for the quantification of traces of elements of interest in a wide range of samples such as metallic alloys, soils, liquids, and air.

The objective of this work was to construct an analytical formula to fit the line profiles measured from plasmas with typical temperatures and electron densities of 1 eV and $(10^{16}–10^{17})$ cm^{-3}, respectively. To this aim, the different physical mechanisms affecting the emissivity line profiles (i.e. background due to continuum, self-absorption, self-reversal, asymmetry, and noise) were taken into account. Our approach was based on a pseudo-Fano function and it will be useful to 1) generalize the expression due to Kielkopf and Allard [6] to Voigt profiles when the Gaussian component, given by the Doppler broadening and/or the monochromator slit, is important; 2) avoid the problem of solving a convolution integral; and 3) further extend the treatments of Zwicker [2] and Cowan-Dieke [11] for the cases when the self-absorption dip is not coincident with the emission peak. Moreover, the emissivity profiles can be retrieved from the fitting of the experimental lines. The validity of the proposed model was verified by determination of the relative gA values of five Co I lines which was compared with those reported in NIST database [12].

2. Line profile for an arbitrary optical thicknesses

The spectral line profile with an arbitrary optical thickness τ can be written in several equivalent forms. Starting from the general expression in terms of the emissivity$\varepsilon(\omega)$ and the opacity $\kappa(\omega)$ for a homogeneous slab of thickness L, and integrating along the line of sight it results [7]

$$I(\omega, L) = \frac{\varepsilon(\omega)}{\kappa(\omega)}\{1 - \exp[-\kappa(\omega)L]\}; \quad (1)$$

where $\varepsilon(\omega)$ and $\kappa(\omega)$ are both proportional to the normalized emissivity line profile $P(\omega)$. As one of the authors has shown in Reference [8], when $P(\omega)$ is Lorentzian, $I(\omega, L)$ can be put in terms of the

* Corresponding author.
E-mail address: ddiaz@exa.unicen.edu.ar (D.D. Pace).

[1] In laser produced plasmas, the lines become narrower at later times (microseconds or higher) and in this scenario Stark effect is negligible.

http://dx.doi.org/10.1016/j.sab.2017.07.005
0584-8547/

optical thickness $\tau(\omega, L) = \kappa(\omega)L$ and, in order to have an intensity profile normalized to unity, it must have the following functional form

$$I(\omega, \tau_0) = \frac{\left\{1 - \exp\left[-\tau_0 \frac{\gamma^2}{(\omega^2+\gamma^2)}\right]\right\}}{\pi\gamma\tau_0 M\,(1/2, 2, -\tau_0)}, \tag{2}$$

being τ_0 the maximum optical thickness which is a combination of universal constants as well as source parameters (N_i, L, T, etc.) [8], γ the *HWHM*, and $M(1/2, 2, -\tau_0)$ a confluent hypergeometric (or Kummer) function. Expanding Eq. (2) in series up to first order around τ_0, we have

$$I^{thin}(\omega) = \frac{\gamma}{\pi(\omega^2 + \gamma^2)} \equiv \mathcal{L}(\omega), \tag{3}$$

which is a Lorentzian function normalized to the unity. Then, Eq. (2) can be put, in general, in terms of the thin line profile $I^{thin}(\omega)$:

$$I(\omega, \tau_0) = \frac{\left\{1 - \exp\left[-\tau_0 \gamma\pi I^{thin}(\omega)\right]\right\}}{\pi\gamma\tau_0 M\,(1/2, 2, -\tau_0)} \tag{4}$$

The profiles given by Eq. (2) or (4) refer to spectral sources that, eventually, can lead to self-absorption, when $\kappa(\omega)L \gtrsim 1$ [7,9].

It should be noted that for individual profiles could be convenient to use normalized profiles, as given by Eq. (2) or (4). On the other hand, when comparing different lines such normalization does not make sense and it is better to rewrite Eq. (4) as

$$I(\omega, \tau_0) = Constant \times \left\{1 - \exp\left[-\tau_0 \gamma\pi I^{thin}(\omega)\right]\right\}, \tag{5}$$

being *Constant* a scale factor.

3. The generalized Voigt profile

The Voigt profile $V(x)$ is the convolution of a Gaussian, $\mathcal{G}(x)$, with a Lorentzian, $\mathcal{L}(x)$. The corresponding expressions normalized to the unity are, for lines centered at $x = 0$ (to simplify the notation; later, it can be changed to $x - x_0$)

$$\mathcal{G}(x) = \frac{1}{\sqrt{\pi} w_G} \exp\left[-(x/w_G)^2\right] \tag{6}$$

being $w_G = \gamma_G/\sqrt{\ln 2}$ and γ_G the corresponding HWHM. Analogously

$$\mathcal{L}(x) = \frac{1}{\pi w_L} \frac{w_L^2}{x^2 + w_L^2} \tag{7}$$

with $w_L = \gamma_L$. Calling $a = w_L/w_G$, we can write $V(x)$ in the form

$$\mathcal{V}(x) = \frac{a}{\pi^{3/2}} \int_{-\infty}^{\infty} \frac{\exp\left[-((x - x')/w_G)^2\right]}{x'^2 + w_L^2} dx'. \tag{8}$$

To take into account that the plasma could be optically thick ($\tau > 1$) and, additionally, with a possible external colder region, in such a way that self-reversal be possible and, at last, a possible asymmetry due i.e. to the ionic density, the convolution integral can be generalized in the form

$$V(x) = Constant \times \int_{-\infty}^{\infty} e^{-[(x'-x)/w_G]^2} \left[1 - e^{-\tau_0\gamma^2/(x'^2+\gamma^2)}\right] \times (1 + B_{asym}x')\, e^{-\frac{A_{auto}w_a^2}{(x'-d_a)^2+w_a^2}} dx'. \tag{9}$$

In the above equation we have 1) the Gaussian Kernel to convolve:

$$\exp\left(-[(x' - x)/w_G]^2\right),$$

2) the profile $I(\omega)$ given by Eq. (5), 3) the asymmetry term $(1 + B_{asym}x')$, and 4) the self-reversal term:

$$\exp\left[-A_{auto}w_a^2/\left((x' - d_a)^2 + w_a^2\right)\right],$$

where w_a is the HWHM of the self-reversal profile occurring at the position d_a.

From a practical point of view, fitting an experimental line by using the previous convolution integral, i.e. Eq. (9), is very cumbersome. Therefore, we postulate in the following section an analytical function that allows a relatively simple fit of measured line. The last step will be to recover the emissivity line, with no asymmetry ($B_{asym} = 0$), with no self-absorption ($A_{auto} = 0$) and also $\tau \ll 1$. This will make feasible the estimation of the relative *gf* values and its well known applications to the spectrometry.

4. Fano and pseudo-Fano profiles

Fano (or Beutler-Fano) profiles, $F_q(x)$, had been widely used for auto-ionization studies [4], as well as in applications in a multitude of physical systems [10]. $F_q(x)$ is given by an expression of the type

$$F_q(x) = \frac{A(x + q)^2}{(x^2 + w^2)}. \tag{10}$$

The maximum value of Eq. (10) occurs when $x = w^2/q$, whence $F_q(w^2/q) = A(q^2 + w^2)/w^2$ and, when $q = 0$, $F_0 = A$. the minimum occurs when $x = -q$, $\therefore F(-q) = 0$. The case $q = 0$ produces a typical symmetrical *absorption* profile; for other q values, the profile is highly asymmetrical, unless for $q \to \infty$ in that the profile becomes symmetrical. The width of the curve $F_q(x)$ is $FWHM = 2w$.

As in this work we are interested in *emission* lines, with probable contributions due to the self-absorption of the source as well as probable self reversal due to absorption by cooler outer region [7,9], we modify the previous expression as follows:

$$F(A, q, w; x) = A\left[1 - \frac{(x + q)^2}{(x^2 + w^2)}\right], \tag{11}$$

in such a manner that when $q = 0$ we have a Lorentzian curve:

$$F(A, 0, w; x) = \frac{Aw^2}{x^2 + w^2}, \quad F(A, 0, w; 0) = A. \tag{12}$$

Eq. (11) is a very reasonable generalization of the Lorentzians and, therefore, can be a good description of Voigtian curves when $w_L >$

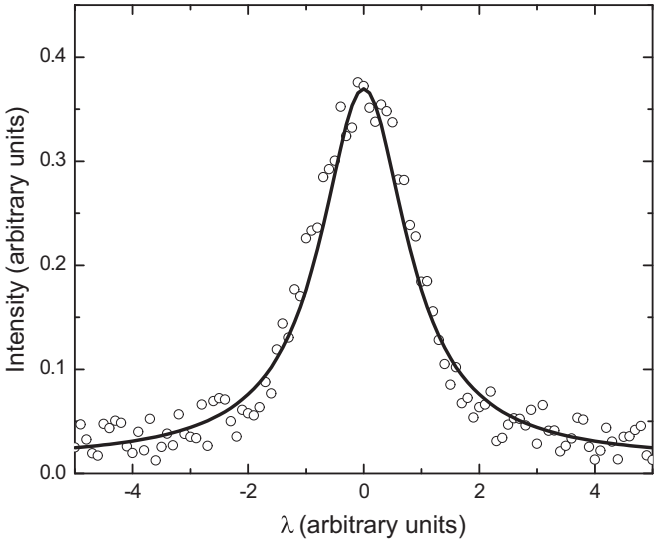

Fig. 1. Synthetic Voigt profile with $a = w_L/w_G = 0.5$ (basically a Gaussian) with added noise (open circles). The line is the fit using our approach, with $p = 0$.

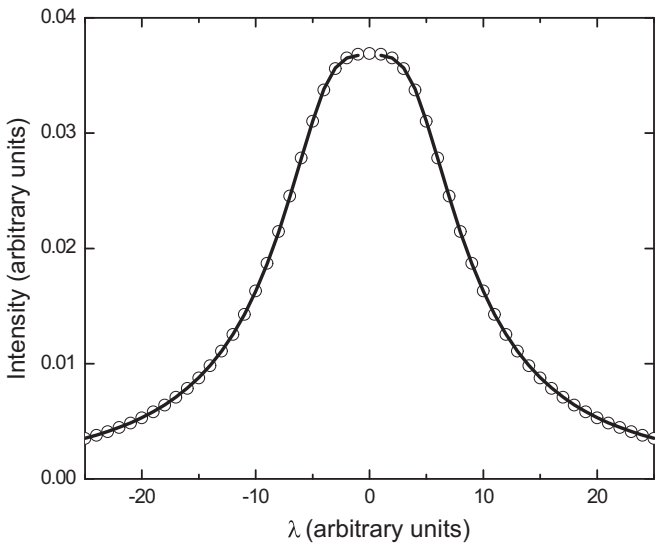

Fig. 3. Synthetic profile without dip ($A_{auto} \approx 0$). The points are the values after Eq. (9) whereas the lines are the fits according to our approach, with $p = 0$.

w_G, eventually asymmetrical, until now with no self-absorption, which will be accomplished in a later section.

A better generalization of Eq. (11), also useful when $w_L < w_G$ is

$$F^{thin}(A, q, w; x) = A\left\{1 - \left[\frac{(x+q)^2}{(x^2+w^2)}\right]^p\right\} \tag{13}$$

with $p \approx 1$, because this gives a better fit in the wings of the Voigtians. Examples showing that our formula (Eq. (13)) can reproduce Voigt profiles with different values of w_G/w_L are presented in Figs. 1 to 2. This shows the superiority of Eq. (13) with respect to Eq. (11).

Additional examples of synthetic profiles, now generated using Eq. (9), are shown in Figs. 3–5.

5. The construction of our formula

From the two previous subsections, specially Eqs. (4) and (13), we make the proposal that if a line could reach self-absorption ($\tau_0 \gg 1$) and could have a certain asymmetry (i.e. due to ionic broadening), then its intensity profile can be described by a pseudo-Fano function of the form

$$F(\ldots) = B\left\{1 - \exp\left[-A\left(1 - \left(\frac{(x+q)^2}{(x^2+\gamma^2)}\right)^p\right)\right]\right\} \tag{14}$$

where A plays the role of τ_0 (as we will see in §5.1) and B is a scale factor, q measures the asymmetry, γ gives the *HWHM* of the recovered emissivity line. In real spectra x should be substituted by $(x - x_0 - d)$

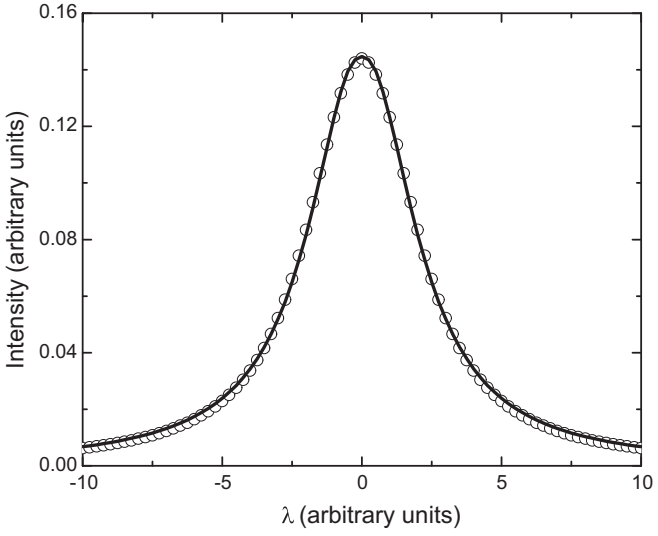

Fig. 2. Synthetic Voigt profile with $a = w_L/w_G = 2$ (basically a Lorentzian). The points are the values after Eq. (9) whereas the lines are the fits according to our approach, with $p = 0$.

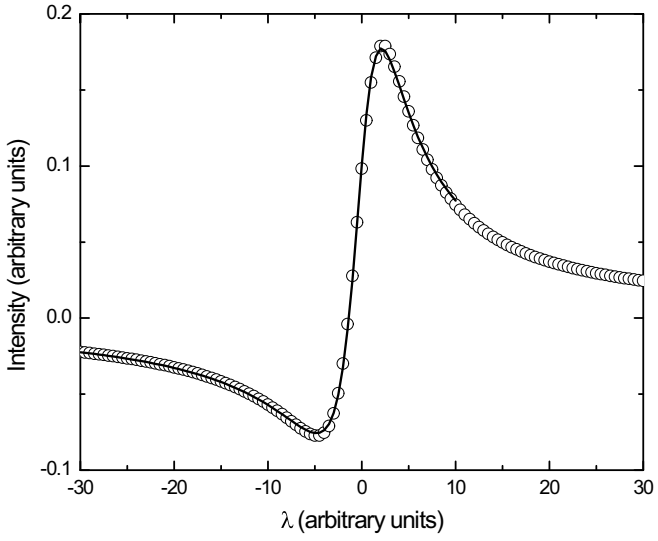

Fig. 4. Synthetic asymmetric profile, multiplied by $(1 + 0.75x)$, with no self-absorption. The points are the values after Eq. (9) whereas the lines are the fits according to our approach, with $p = 0$.

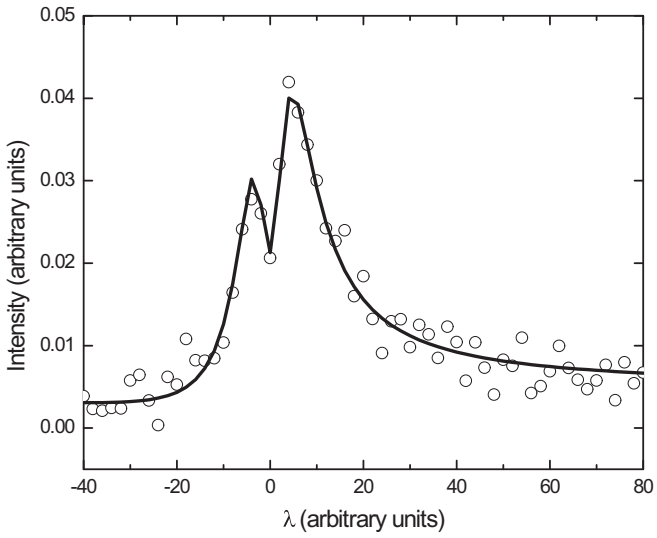

Fig. 5. Synthetic asymmetric profile, with self-absorption and noise. The points are the values after Eq. (9) whereas the lines are the fits according to our approach, with $p = 0$.

where d is the possible shift by plasma effects [1] and x_0 indicates the non-perturbed position of the line.

Based in the previous work of Kielkopf and Allard [6], we must add the self-reversal factor, due to the external cooler plasma, whereas the self-absorption occurs in a position d_a

$$F_{abs} = \exp\left[-\frac{A_{auto} w_a^2}{(x-d_a)^2+\gamma_a^2}\right]; \tag{15}$$

which generalize the classical treatments of Bartels [2] and of Cowan-Dieke [11], for which the dip is at $d_a = x_0$.

Finally, we write a general expression for the line profile as a function of several parameters$A, B, q, \gamma, d, A_{auto}, p, \gamma_a, d_a, C$ (x_0 is known from tables)

$$F\left(\{A,B,q,\gamma,d,A_{auto},p,\gamma_a,d_a,C\},x\right) =$$

$$= C + B\left\{1-\exp\left[-A\left(1-\frac{(x+q)^2}{x^2+\gamma^2}\right)^p\right]\right\}\exp\left[-\frac{A_{auto}w_a^2}{(x-d_a)^2+\gamma_a^2}\right]. \tag{16}$$

Before applying our proposed formula (Eq. (16)) to experimental lines, we have verified that it describes a wide range of possible emission profiles. Such verifications are presented in Figs. 1–5, as was mentioned above. It should be mentioned that, despite the apparently high number of parameters, several of them can be readily estimated from the experiment, and later released if necessary, as explained immediately in §6. In many cases of lines obtained by Laser Produced Plasmas, only four parameters are generally needed.

5.1. A plays the role of τ_0

In the case of a line given by the Eq. (5) the peak intensity is, when there is no self-absorption

$$I(0,\tau_0) = Constant \times \{1-\exp[-\tau_0]\},$$

Table 1
The results for the parameters corresponding to the transition λ = 340.5 nm, after the maximum likelihood estimation using the Monte Carlo Markov chain method.

Variables	θ_0	Marginal median	Credibility interval
A	0.1369	0.1393	[0.12,0.17]
q	0.0092	0	[−0.0103, 0.0102]
ϖ	0.1274	0.1312	[0.11,0.18]
d	0.0584	0.0584	[0.57,0.59]
A_{auto}	0.4176	0.4103	[0.319,0.421]
ϖ_a	0.0370	0.0325	[0.02,0.12]
d_a	0.0218	0.0218	[0.021,0.0225]
C	$9e-9$	0.003	[0,0.0065]

whereas, in our formula, when the thin profile is recovered, that is, when $d = 0, q = 0, p = 1, A_{auto} = 0, d_a = 0$, it turns out that

$$F(x_0) \to B[1-\exp(-A)],$$

whereby, we can establish

$$Constant \times \{1-\exp[-\tau_0]\} = B[1-\exp(-A)],$$

and identify $A = \tau_0$. Keep in mind that, when the profile is normalized, then $B = 1/[\pi\gamma\tau_0 M(1/2,2,-\tau_0)]$ but, given the different relative intensities of the transitions, no normalization must be considered here. Therefore, B is a scale factor, taking into account the experimental parameters, such as setup, electronic gain, and detector response.

6. Fitting methodology

To fit measured spectral lines under the developed approach, the values of some parameters should be firstly estimated. To this aim, the following steps were carried out:

1) C (the background) is obtained by fitting the continuum near the emission line.
2) If the curve is clearly symmetric, then $q \simeq 0$; when released to $q \neq 0$, its sign will depend of the asymmetry: to the right or to the left.
3) The HWHM given by γ can be bounded, because the experimental width will be always greater than the true (thin) width (due to self-absorption).
4) If there are no clearly visible dip, $A_{auto} \approx 0$.
5) The values for d and d_a were set by simple visualization.
6) The optical thickness is given by A; if the flattening is not evident, then $A \gtrsim 0$.
7) p will have an approximate value near to the unity ($p \gtrsim 1$).

6.1. First methodology: fitting four parameters through a least-squares iterative fitting algorithm

The analysis of the line profiles was carried out based in modeling emission line profiles within the framework of our Eq. (16), corresponding to a plasma composed (eventually!) of two regions: a core with a higher temperature surrounded by a periphery with a lower one. Each region of the plasma was pictured as a homogeneous piece in local thermodynamic equilibrium (LTE) characterized by its own set of plasma parameters and for which the model can be applied. The values of the plasma parameters inside these regions are averaged values of the real spatial distributions.

In this approach, the emission intensities of a spectral line was calculated and matched to their experimental profile through a least-squares iterative fitting algorithm, based on the calculus of the

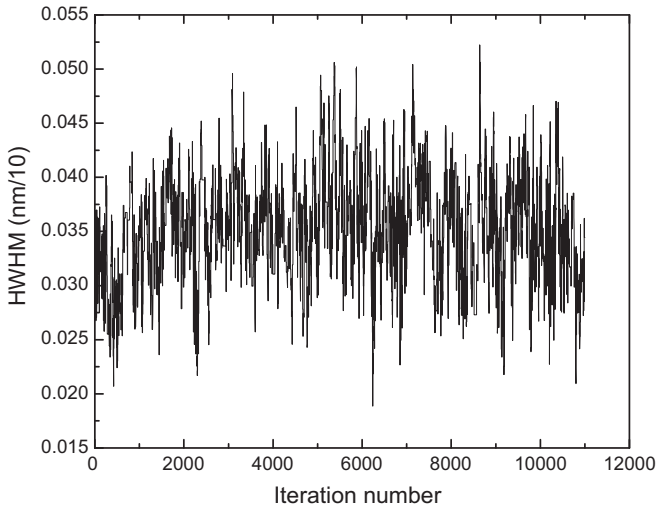

Fig. 6. An example of a converged chain.

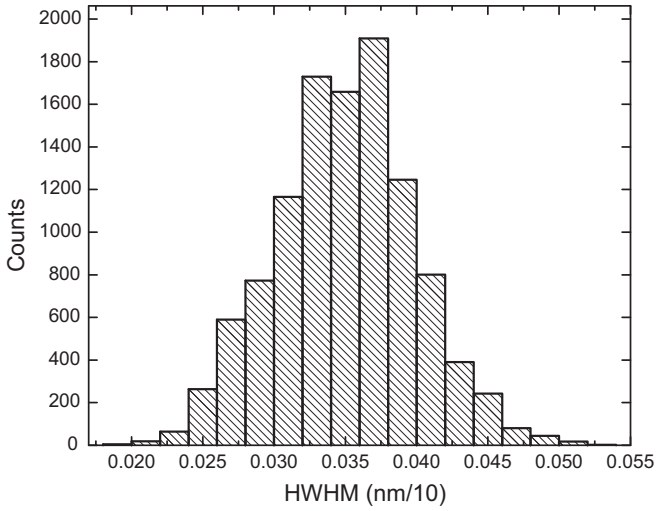

Fig. 7. A resulting marginal histogram (i.e. a histogram of only one variable).

optical thickness for the core and the periphery regions. The optical thickness was represented by a pseudo-Fano functions, whose Lorentzian width is dominated by Stark broadening while the Gaussian width is associated to the instrument profile plus Doppler broadening contributions. Self-absorption can be quantified and subsequently compensated to retrieve the optically thin line profiles.

The fitting procedure was executed systematically for all the Co I lines measured. The inputs are the experimental line and its spectroscopic data available at the NIST Database. The parameters q, d, da, B, and C are not fitting parameters and they are estimated from the measured profiles. Then, estimated ranges of values for the maximum optical thicknesses; i.e.A, A_{auto}, and the Stark widths; i.e.γ, γ_a, are set by the user (typically, A, $A_{auto} = 0.1$–10, and γ, $\gamma_a = 0.01$–0.20 nm in our experiment). Then, by varying these four independent parameters the fitting routine is run until the deviation of the synthetic from the experimental spectrum is minimized and, hence, the profile that reproduces the measurements is obtained along with its wavelength-dependent optical thicknesses. In this way, the output data are the maximum values of the optical thicknesses and the Stark widths for the core and the periphery regions, the total intensity of the line, and the intensity in optically thin conditions.

6.2. Second methodology: a Bayesian analysis; the role of the noise statistics

The so-called least square estimation(LSE) is a technique commonly used to retrieve hidden parameters given a set of measurements through the following expression

$$l(\theta, y) = ||f(\theta) - y||^2 \tag{17}$$

where f is the model, θ is the hidden (or objective) parameter and y is the data or measurement set. As an example, widely known by spectroscopists, a set of bell-shaped experimental points could be fitted by Gaussian, Lorentzian or Voigtian profiles. However, when the influence of the noise is high, LSE may fail, leading to useless results. A classic example of this can be seen in the Deconvolution problem [14]. Given that we may have an instrument response function(IRF) and a convoluted signal (S), the presence of noise makes reconstruction of the underlying signal (o) a problem which can not be tackled with LSE, even when we have the analytical solution of the problem

$$o = \mathcal{F}^{-1}\left\{\frac{\mathcal{F}\{S\}}{\mathcal{F}\{IRF\}}\right\} \tag{18}$$

where $\mathcal{F}$ is the Fourier Transform. This is caused by the fact that many signal can be convoluted with the IRF and produce very similar results. So similar, that LSE can not "see" the true value leading to unphysical solutions. From a classical point of view, to solve LSE is equivalent to solve the so-called maximum likelihood estimation(MLE) problem. In MLE, the main question to be answered is as follows: *given a measurement y, and a model f, which is the value of θ that maximizes the likelihood*?, or, *which is the value of θ that makes the model resemble more the data*?. The likelihood can be stated as [13]

$$p(y|\theta) \propto \frac{\exp\left(-\frac{1}{2}||f(\theta) - y||^2\right)}{Z} \tag{19}$$

with Z the normalization constant that makes the likelihood have a integral of one. The philosophy of the question shows us the underlying problem of both, LSE and MLE, we have to *trust* in the data. In some situations, we can do this but, as in the deconvolution example, this will eventually lead us towards failure.

Situations like deconvolution fell in a branch of mathematics named *inverse problem theory*, which aimed to solve problems of this nature. The main characterization was given by Hadamard [22] who stated the three situations that can lead to get an inverse problem. Namely, if we have a function (model) f, data y and unknown θ and occurs any of the following:

- $f(\theta) = b$ has a solution.
- That solution is unique.
- The solution depends continually in the data, then we are in the presence of an inverse problem.

In other words, what we are saying is that our model is not injective (different values of θ produces the same value of y - $y = \theta^2$, for example) or it is too sensitive of small variations, meaning that little changes in y will produce big changes in θ. This is the main problem with measurements. There will always be noise which produces little changes in the measurement, leading to an inverse problem. To suggest a solution, Tikhonov regularization(TR) [14] can be used. However, we will use a more powerful technique which allow us to

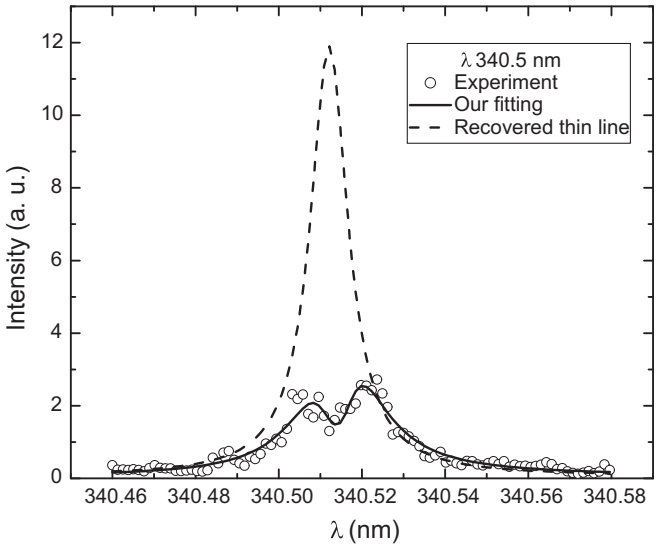

Fig. 8. Line $\lambda = 340.5$ nm obtained through the LIBS technique, showing the characteristic dip of a strongly absorbed line from an inhomogeneous plasma. The full line indicates the fit using our approach, with $p = 1.1$, whereas the dashed line shows the recovered thin line.

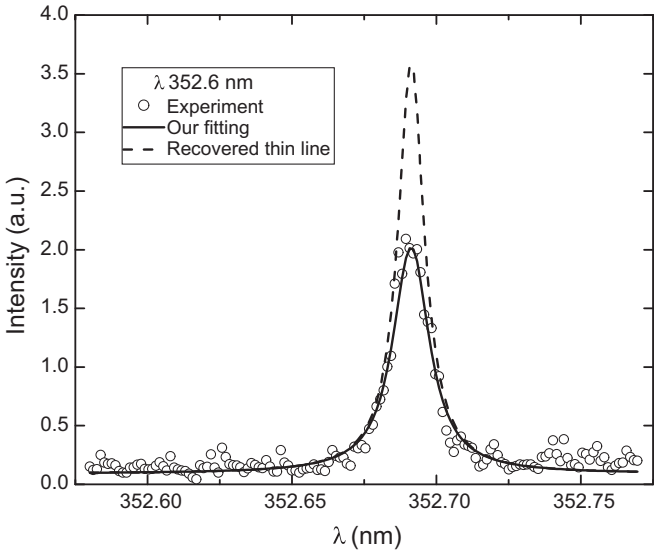

Fig. 9. Line $\lambda = 352.6$ nm obtained through the LIBS technique. The full line indicates the fit using our approach, with $p = 1$, whereas the dashed line shows the recovered thin line.

recover more information than TR and deterministic counterparts. Bayesian analysis relies on probability and statistics theory and is a tool which gives relation between two events. If A, B are two events of interest, Bayesian Theory states, in classical terms, that if $p(A)$ is the probability that event A occurs, $p(A|B)$ is the probability that event A occurs given B occurred and $p(A|B)p(B)$ is the probability that **both** events A**and**B occur, then $p(B|A)$ is the probability that event B occurs given A occurred:

$$p(B|A) = \frac{p(A|B)p(B)}{p(A)}. \tag{20}$$

As an example, let us consider the following situation: let A and B denote the events *the patient presents a set of symptoms, cough, fever, etc* and *the patient has a flu*, $p(A)$ is the probability that the patient has the symptoms, $p(B)$ is the probability that the patient has a flew and $p(A|B)$ is the probability that the patient presents the symptoms given that he has a flew. From the classical point of view, this probabilities would be estimated from general databases, but this information is synthesized and does not take into account particular information that could be of interest for the doctor.

But, being Bayes theorem deduced from the postulates of the Probability Theory, a new point of view was introduced in the last years: the subjective probability or, in other words, the scientific reasoning in conditions of uncertainty. Bayes theorem is an amazingly powerful tool, because it allow us to relate causal and inversely causal events, as long as we are able to code them through probability functions. This is the main tool used in Bayesian Analysis to perform *inference* [15], i.e. to discover what event B produced A. As can be seen in Eq. (20), there are four ingredients needed. Namely, the *likelihoodp*$(A|B)$ which relates the events A and B by telling us how likely A and B are, the *evidencep*(A) which tells us how likely the event A is to happen, the *prior informationp*(B) where we can say *what we do know* about the event B, which is the variable of interest and, finally, the *posterior distribution* where all this information is coded and tell us *what is the distribution of the event B given that event A happened*?

Following with the example of the doctor, $p(A)$ stands for the evidence (the patient arrived with probability different from zero of having a flew), $p(B)$ stands for the prior information (the doctor know the patient and the environmental context) and $p(A|B)$ stands for the likelihood, the symptoms make likely to have a flew, and that is what the doctor learned in Medical School. The main difference with the classical approach lies in how do we calculate the probabilities. We may use the information of databases, but there are several factors that may not be taken into account by statistics and that the doctor considers important when he has to make a diagnosis. As an extreme example of this would be in the situation when we face an illness that is so rare that there may be only a few documented cases, or in the presence of a new illness. Let us suppose that we only had 20 documented cases of such illness, the statistics may not be very reliable (in the sense that large variance may be expected). But, if we get to contact a specialist in the illness, who may have been in contact with some of the patients who had this rare disease, he may be more useful in the sense that he may be able to "see" things that a regular doctor may not have seen given his experience and the novelty of this disease.

To lead Bayes theorem towards our application we have to define our events A and B. This is done via random variables Θ which is the collection of all possible values of our parameters and Y which is the collection of all possible measurements. When we get a measurement the random variable Y gets a specific value, i.e. $Y = y$, when we use a specific value of θ it also instantiates in $\Theta = \theta$. We have a model (in our particular application, the model is Eq. (16)) that relates the hidden parameters θ with the measurement y through the relation

$$p(Y = y|\Theta = \theta) \propto \exp(-||f(\theta) - y||^2); \tag{21}$$

the exponent is, exactly, the operator used in LSE, and here is where we can see how Bayesian Theory generalizes LSE. This is also the likelihood used in MLE (and this is why both methods are equivalent, minimizing the exponent is the same that maximizing the likelihood). The likelihood, stated this way, obtains information through the statistics of the noise which, depending of the acquisition devices, can be stated as normal. The main advantage of Bayes Theorem is the prior information term, where we can code knowledge previously acquired or predicted by theory, physical behaviour, etc. A canonical example is to use a Uniform distribution over the variables θ_i. This distributions assigns the value 1 when θ is in an interval $[a, b]$ and 0 otherwise. This distribution does not assign any

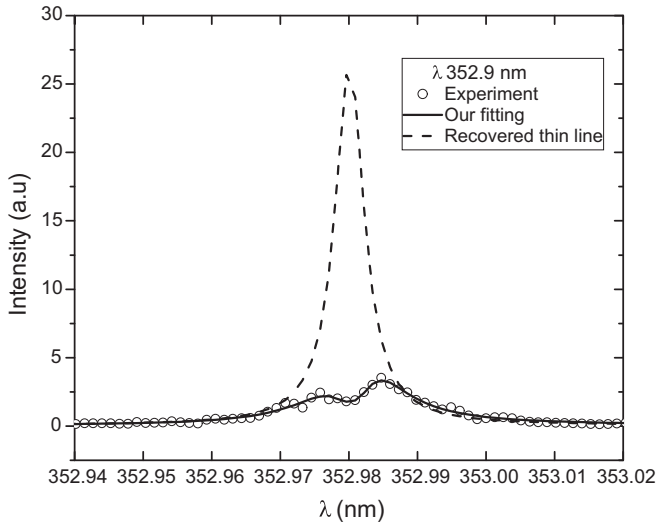

Fig. 10. Line $\lambda = 352.9$ nm obtained through the LIBS technique. The full line indicates the fit using our approach, with $p = 1.25$, whereas the dashed line shows the recovered thin line.

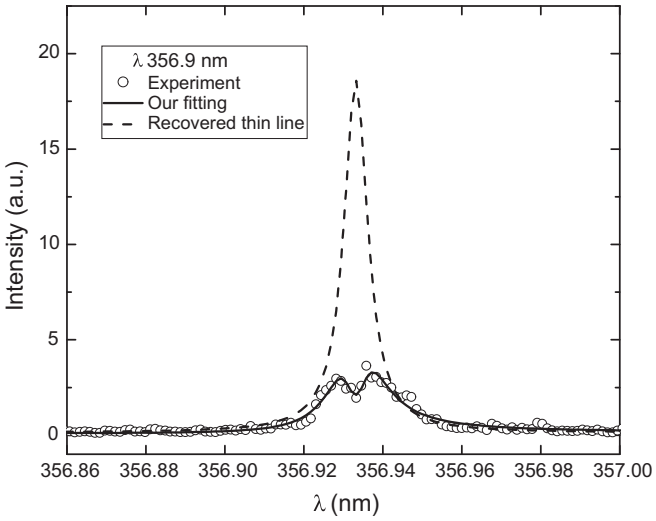

Fig. 11. Line $\lambda = 356.9$ nm obtained through the LIBS technique, recorded in the plasma nucleus. The full line indicates the fit using our approach, with $p = 1$, whereas the dashed line shows the recovered thin line.

special weight to values inside the interval, which means that every point inside the interval is as probable as any other. This density is useful in establishing bounds, and we can use them when we only know bounds. Another useful density is the Normal Distribution, where we state that we know that our variable is more likely to be near the mean, and with 99.74% probability, within the interval $[\mu - 3\sigma, \mu + 3\sigma]$. The knowledge of the distributions helps us set the values of the parameters (a, b in the Uniform, μ, σ in the Normal) and an analysis must be performed in order to choose. We have shown two examples of prior distributions, but we can combine them (Uniform × Normal) or use another kind of distribution depending of the variables. The evidence is not easy to get, because we will need good integration skills and can be very difficult in highly dimensional spaces (i.e. when we have many unknown variables). But this will not be a problem because the method of Monte Carlo Markov chain [14,16] (MCMC) does not need the evidence $p(A)$ (see Eq. (20). And this is the last tool needed to perform this Bayesian Analysis, which is the study of the posterior distribution. If we had an analytical posterior, we could calculate the mean, the median, the mode, etc, which would give us *point estimates*. This estimates are used to summarize in a single value, all the information of the distribution. More information can be obtained from *interval estimates*, which give us information such as *the probability that the value x lies in the interval* $[c, d]$ *is p-percent*. This kind of information is crucial, because we get a tool to analyze the performance of our methods (experimental and processing). In general, there is no hope of getting analytical posteriors, and this is where MCMC enters. MCMC is a numerical technique used to explore a given distribution (even in non-Bayesian analysis), it starts in an initial distribution and advances iteratively until it reaches the objective distribution, once there it moves and return a sample that represents the entire objective distribution. In a certain sense, it is a procedure similar to what we do with a known distribution. If we generate random samples from, for example, a Normal, Uniform, Gamma, Exponential, etc distribution and then we generate a histogram with the random samples, we get something that resembles the distribution that generated the data, and we could perform an analysis using that sample. MCMC does exactly the same but it can work in *any* distribution. The only disadvantage is that, depending on the nature of the objective distribution, it can be computationally expensive. At the end of the procedure we get a sample where we can perform an analysis (for example, calculate the mean) and we get the mean of the posterior distribution, or we can calculate marginal confidence intervals, to see each variable apart.

In this work, we have used the likelihood stated in Eq. (21), the a priori distribution is a normal distribution for each variable (i.e. assuming they are mutually independent), finally getting

$$p(\Theta = \theta | Y = y) \propto \exp(-||A(\theta) - y||^2) \times \prod_{i=1}^{10} N(\theta_i; \mu_i, \sigma_i) \tag{22}$$

where $\prod_{i=1}^{10} N(\theta_i; \mu_i, \sigma_i)$ is a product of normal density distributions of mean μ_i and standard deviation σ_i, and MCMC was used to get the results shown in Table 1. In Figs. 6 and 7, an example of a converged chain is shown and a resulting marginal histogram (i.e. a histogram of only one variable) is shown. This information is used by an analyst to perform whether our information state has improved and how it did improve.

This sub-problem can be tackled with any optimization toolbox, in this work, we used a multi-start algorithm finding the MLE [13,14] . Once we have obtained the MLE, we use it as an initial point for a MCMC run. As an example, we show in Table 1 the results for $\lambda = 340.5$ nm (with $p = 1$).

The moral of this methodology is that, when we are in the presence of a complicated model f given, in our case, by the Eq. (16), a good practice is to start with a LSE iterative fitting and use the retrieved parameters in a posterior Bayesian analysis.

6.3. Applications

In order to evaluate the validity of the method, our proposed formula (Eq. (16)) was applied to experimental lines recorded from two different plasmas types: 1) laser generated plasmas on metallic alloys [17], and 2) pinch discharges with relatively high peak currents (up to 1 kA) in capillaries tubes [21]. In the first case, the transitions recorded were resonant or near-resonant that showed notorious dips as well as small asymmetries. Hence, the plasma plume can be figured out as composed by a hotter central region surrounded by a colder external one. In the experiment, a pulsed Q-switched Nd:YAG laser ($\lambda = 1064$ nm) with pulse width of 7–8 ns and a repetition rate between 1 and 20 Hz was focused on the metallic alloy with a lens of 10 cm focal length. The detection system consisted in a monochromator Jovin-Yvon with a resolution of 0.01

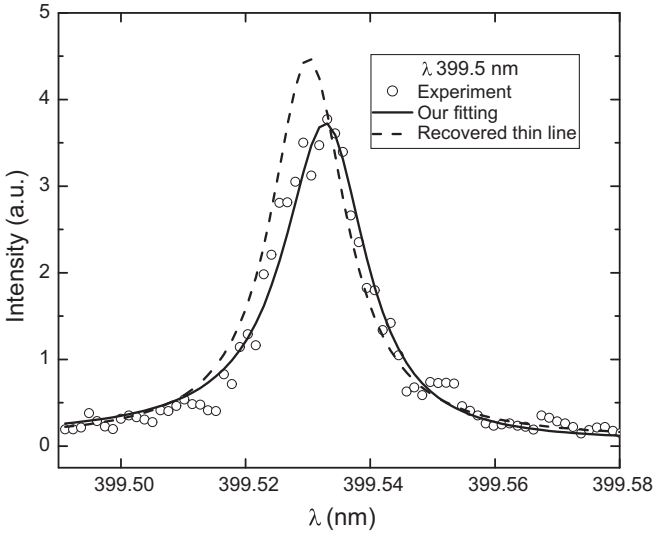

Fig. 12. Line $\lambda = 399.5$ nm obtained through the LIBS technique; a peak shift is observed. The full line indicates the fit using our approach, with $p = 1$, whereas the dashed line shows the recovered thin line.

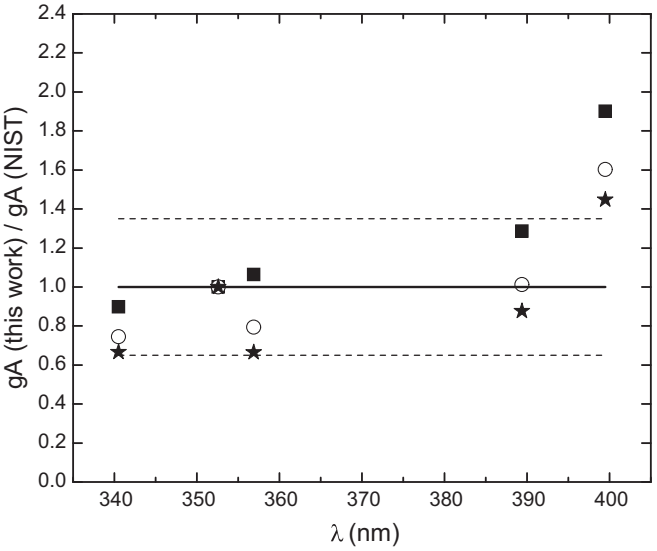

Fig. 13. The ratio between our *gf* values and the corresponding NIST ones, for $kT = 0.75$ eV. Dotted lines indicate ±30% deviations (the sum of the respective relative errors, of the order of 15% [12]). The squares indicate $kT = 0.75$ eV, the circles $kT = 1.00$ eV and the stars $kT = 1.25$ eV.

nm (at 300 nm), with a slit width of 40 μm and a photomultiplier Hamamatsu IP28. The signal was processed by a gated integrator and boxcar averager triggered externally from the laser Q-switch output at a delay time of 1.5 μs and a gate width of 30 ns. In the second case, the lines measured showed clears broadenings and asymmetries. The experiment was carried out with a pyrex tube of 3 mm internal diameter with two tungsten electrodes 80 cm apart. The gas pressure was maintained between 0.06 and 0.5 mbar by employing a conventional vacuum system. The excitation was obtained by discharging a capacitor of 40 nF charged up 12 kV giving us a peak current between 140 and 1000 A. The current was observed by using a Rogowski coil and indicated a pulse oscillation period of 2.5 μs. The monochromator and the boxcar were the same as above.

After obtaining the fitted parameters, the thin lines were recovered making $C = 0$, $A \ll 1$, $d = 0$, $q = 0$, $p = 1$, $d_a = 0$ and $A_{auto} = 0$. If $A_{auto} = 0$, we do not need the values of γ_a and we can make with impunity $\gamma_a = 1$). Then, the peak of the recovered line $F(A, B, 0, \gamma, 0, 0, 1, 1, 0, 0|x) = BA$ (making $A \ll 1$). As examples, in Figs. 8–12 we show the experimental, the fitted and the recovered profiles for five Co I lines. Additionally, in Fig. 14, the strongly asymmetric line 508.0 nm corresponding to Xe II spectrum, obtained in high current capillary discharges is shown.

7. Transition probabilities of Co I lines

The transition probabilities A_{ji} (or the related oscillator strengths f_{ji}) are important spectroscopic quantities for modeling of both astrophysics and laboratory plasmas.In this work, we measured five Co I lines measured by LIBS technique. The spectroscopic parameters were taken from NIST Database, where the probability transitions have an accuracy of 18–25%. In our work we have considered the lines with $\lambda/\text{nm} = 340.5, 352.6, 356.9, 389.4$ and 399.5, obtained with the LIBS technique, with the electron temperatures estimated (in first instance) in the range $kT = 0.50 - 1.25$ eV [17]. In the ideal regime under thin and LTE conditions, the g_iA_{ik} value for a transition $i - k$ respect to another transition $j - l$ is given by [7]

$$g_iA_{ik} = g_jA_{jl}\left(\frac{I_{ik}}{I_{jl}}\right)\left(\frac{\omega_{ik}}{\omega_{jl}}\right)\exp\left[-(E_j - E_i)/kT\right]; \quad (23)$$

where the intensity ratio can be experimentally obtained from the corresponding areas under the recovered thin profiles and the g_jA_{jl} values for the reference transition is taken from NIST Database. In our case, the line 352.6 nm ($g_jA_{jl} = 1.3 \times 10^8 s^{-1}$) was selected as reference and the g_iA_{ik} values were calculated for the other 4 lines. The mean values and their corresponding dispersion are, for different temperatures the following: for $kT = 0.50$ eV: 1.96 ± 0.72, for $kT = 0.75$ eV: 1.36 ± 0.48, for $kT = 1.00$ eV: 1.14 ± 0.40 and for $kT = 1.25$ eV: 1.03 ± 0.37. From the above values, we consider that it is reasonable to discard the value $kT = 0.50$ eV. Indeed, the coexistence of *Co I* and *Co II* lines would indicate that a value $kT = (1.00 \pm 0.25)$ eV is in accordance with preliminary estimates based in Saha's relationship. We see that, for the above temperature range, the ratio $g_iA_{ik}|_{our}/g_iA_{ik}|_{NIST} \approx 1$ for four of the five lines (see Table 2 and Fig. 13). Although two of us (DDP and HODR) were co-authors of some works using the self absorbed lines [18–20], we think that our present work can be a complement to that approach.

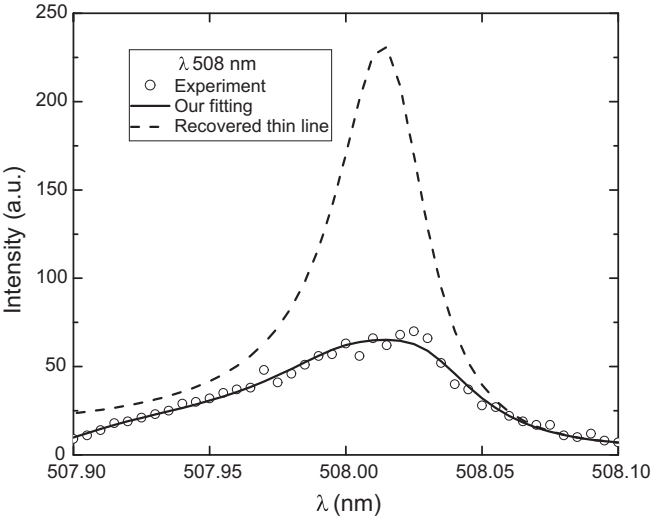

Fig. 14. The strongly asymmetric line 508.0 nm corresponding to Xe II spectrum, obtained in high current capillary discharges (see text for experimental details). The full line indicates the fit using our approach whereas the dashed line shows the recovered thin line.

Table 2
The comparison between the *gA* values tabulated in the NIST repository [12] and our values, for five lines of Co I. The superscripts indicate the three considered temperatures: 0.75, 1.00 and 1.25 eV.

λ/nm (Co I)	gA_{NIST}/s^{-1}	$gA^{0.75}_{our}/s^{-1}$	$gA^{1.00}_{our}/s^{-1}$	$gA^{1.25}_{our}/s^{-1}$
340.5	1.0×10^9	1.0×10^9	7.5×10^8	6.7×10^8
352.6	1.3×10^8	1.3×10^8	1.3×10^8	1.3×10^8
356.9	1.2×10^9	1.2×10^9	9.5×10^8	8.0×10^8
389.4	5.5×10^8	7.0×10^8	5.6×10^8	4.8×10^8
399.5	2.5×10^8	4.8×10^8	4.0×10^8	3.6×10^8

7.1. Asymmetric lines

In the Reference [21] we used high current pinched discharges to measure *XeII* lines with relatively high gas densities. Increasing one or both, the gas density and/or the peak current, asymmetric profiles and line shifts were recorded. In Fig. 14, the experimental profile and the recovered one are shown. In this case, a Lorentzian emissivity profile can not be assumed because asymmetry and shift of the line are clearly observed.

8. Conclusions

A method for the analysis of line profiles based in the pseudo-Fano function was developed, which results of more simple application than the Voigt function usually employed in Spectroscopy to represent the line shapes. A pseudo-Fano function was constructed which describe properly the different effects occurring in plasma sources and subsequently reflected in the measured profiles. The method was successfully evaluated for Co I lines recorded from a LIBS experiment and for a Xe II line from a high-current pinched discharge. In addition, the optically thin lines were retrieved and used for the determination of the *gA* relative ratios of the Co I lines. With respect to the determination of the plasma temperature, our work can be a complement of the use of self absorbed lines. Overall, the good general agreement found between the proposed model and the experiments demonstrated its suitability for spectroscopic applications.

Acknowledgments

The authors gratefully acknowledge the opinions of both reviewers and the Editor; the paper is clearly improved after the corrections were made. This work was supported by the Consejo Nacional de Investigaciones Científicas y Técnicas (CONICET) and the Comisión de Investigaciones Científicas de la Pcia. de Bs. As. (CIC).

References

[1] H. Griem, Principles of Plasma Spectroscopy, Cambridge University Press, Cambridge, 1997.
[2] H. Zwicker, Evaluation of plasma parameters in optically thin plasmas, in: W. Loche-Holtgreven (Ed.), Plasma Diagnostics, North-Holland Publishing Company, Amsterdam, 1968,
[3] I.I. Sobelman, L.A. Vainshtein, E.A. Yukov, Excitation of Atoms and Broadening of Spectral Lines, Springer-Verlag, Berlin, 1981.
[4] R.D. Cowan, The Theory of Atomic Structure and Spectra, University of California Press, Berkeley, 1981.
[5] J.A. Pomarico, D.I. Iriarte, H.O. Di Rocco, An analytic collisional-radiative model incorporating non-LTE and optical depth effects, Eur. Phys. J. D Atom. Mol. Opt. Phys. 19 (2002) 65–72.
[6] J.F. Kielkopf, N.F. Allard, Shift and width of the Balmer series H_α line at high electron density in a laser-produced plasma, J. Phys. B: At. Mol. Opt. Phys 47 (155701) (2014) 6pp.
[7] A. Corney, Atomic and Laser Spectroscopy, Oxford University Press, Oxford, 1977.
[8] H.O. Di Rocco, F.O. Bredice, V. Palleschi, The calculation of the optical depths of homogeneous plasmas; analytical, experimental and numerical considerations, Appl. Spectrosc. 65 (2011) 1213–1217.
[9] A. Thorne, U. Litzén, S. Johansson, Spectrophysics: Principles and Applications, Springer-Verlag, Berlin, 1999.
[10] A.R.P. Rau, Perspectives on the Fano resonance formula, Phys. Scr. 69 (2004) C10–c13.
[11] R.D. Cowan, G.H. Dieke, Rev. Mod. Phys. 20 (1948) 418.
[12] A. Kramida, Y. Ralchenko, J. Reader, NIST ASD Team. NIST atomic spectra database (version 5.1), National Institute of Standards and Technology, Gaithersburg, MD, 2013.available: http://physics.nist.gov/asd; [Online].
[13] V.K. Rohatgi, Statistical Inference, Courier Corporation. 2003.
[14] J. Kaipio, E. Somersalo, Statistical and Computational Inverse Problems, vol. 160. Springer Science and Business Media, Berlin, 2006.
[15] J.M. Bernardo, A.F. Smith, Bayesian Theory, John Wiley & Sons, Canada, 2006.
[16] D. Calvetti, E. Somersalo, An Introduction to Bayesian Scientific Computing. Ten Lectures on Subjective Computing, vol. 2. Springer, Berlin, 2007.
[17] C.A. D'Angelo, D.M. Díaz Pace, G. Bertuccelli, D. Bertuccelli, Laser induced breakdown spectroscopy on metallic alloys: solving inhomogeneous optically thick plasmas, Spectrochim. Acta B 63 (2008) 367–374.
[18] F. Bredice, F.O. Borges, H. Sobral, M. Villagran-Muniz, H.O. Di Rocco, G. Cristoforetti, S. Legnaioli, V. Palleschi, L. Pardini, A. Salvetti, E. Tognoni, Evaluation of self-absorption of manganese emission lines in laser induced breakdown spectroscopy measurements, Spectrochim. Acta B 61 (2006) 1294–1303.
[19] G. Cristoforetti, E. Tognoni, Calculation of elemental columnar density from self-absorbed lines in laser-induced breakdown spectroscopy: a resource for quantitative analysis, Spectrochim. Acta B 79–80 (2013) 63–71.
[20] D.M. Díaz Pace, R.E. Miguel, H.o. Di Rocco, F. Anabitarte García, L. Pardini, S. Legnaioli, G. Lorenzetti, V. Palleschi, Quantitative analysis of metals in waste foundry sands by calibration free-laser induced breakdown spectroscopy, Spectrochim. Acta B 131 (2017) 58–65.
[21] G. Bertuccelli, H.O. Di Rocco, Interpretation of asymmetric lines of Xe II obtained in pulsed capillary discharges, Phys. Scr. 52 (1995) 257.
[22] P.C. Hansen, Rank-deficient and discrete ill-posed problems: numerical aspects of linear inversion, J. Soc. Ind. Appl. Math (1998.)